Eur. Phys. J. C (2025) 85:159
https://doi.org/10.1140/epjc/s10052-025-13868-w

THE EUROPEAN PHYSICAL JOURNAL C

Regular Article - Theoretical Physics

Overturning and cracking of stellar objects in modified $f(R, \varphi)$ gravity

Adnan Malik[1,2,a], **Attiya Shafaq**[2,b], **Fatemah Mofarreh**[3,c], **M. Farasat Shamir**[4,5,d], **Wedad Albalawi**[3,e]

[1] School of Mathematical Sciences, Zhejiang Normal University, Jinhua, Zhejiang, China
[2] Department of Mathematics, University of Management and Technology, Sialkot Campus, Lahore, Pakistan
[3] Mathematical Science Department, Faculty of Science Princess Nourah Bint Abdulrahman University, Riyadh 11546, Saudi Arabia
[4] National University of Computer and Emerging Sciences, Lahore Campus, Lahore, Pakistan
[5] School of Computing and Mathematical Sciences, University of Leicester, Leicester, UK

Received: 25 December 2024 / Accepted: 23 January 2025

Abstract This study extends the concept of cracking to self-gravitating, spherically symmetric compact objects in modified $f(R, \varphi)$ theory of gravity, where R represents the Ricci scalar, and φ is the scalar potential. In this regard, we consider spherically symmetric spacetime characterized with an anisotropic matter to detect the instabilities of self-gravitating compact objects via cracking and overturning. Further, we construct the general framework to observe the cracking and overturning points by applying the local density perturbation technique to the configuration governed by barotropic equation of state. The effectiveness of this approach is assessed by analyzing its results on the data of Her X-1, SAX J1808.4-3658, and 4U 1820-30 respectively. It is concluded that cracking points appear in the different interior regions of these three stars. Significantly, this study illustrates the effectiveness of the cracking approach by highlighting the regions sensitive to localized density disruptions, offering valuable insights into the structural behavior of compact stars within a modified gravity framework.

1 Introduction

In modern cosmology and astrophysics, significant attention has been directed toward understanding the spatial dynamics of the expanding universe, with numerous theories proposed to explain its current accelerated expansion [1–3]. High-redshift supernova observations provide direct evidence for this acceleration [4], while indirect evidence emerges from large-scale matter distribution studies, such as those involving galaxy clusters [5]. The driving force behind cosmic expansion is dark energy (DE), characterized by a high negative pressure and accounting for approximately 68% of the universe's total energy. Albert Einstein's general theory of relativity (GR) [6] revolutionized our understanding of space, time, and gravity and remains a foundational pillar of modern physics. However, GR exhibits limitations, including its inability to adequately describe strong gravitational fields, explain the accelerating expansion of the universe, or account for dark matter, which is estimated to constitute a significant portion of the universe's mass. Addressing these shortcomings necessitates modifications to the classical theory, inspiring researchers to explore modified theories of gravity (MTG) that offer novel cosmological insights and surpass GR in explaining specific phenomena.

In recent years, MTG have emerged as a compelling area of research in astrophysics. MTG are essential for addressing the limitations of general relativity, particularly in explaining dark matter, dark energy, and extreme gravitational environments like black holes. By extending the Einstein–Hilbert action, these theories offer new insights into cosmic phenomena and potential unification with quantum mechanics. They also provide predictions that can be tested through experiments and observations, advancing our understanding of the universe. Collaborative efforts by cosmologists and astrophysicists have led to the development of several MTGs, including $f(R)$ [7,8], $f(G)$ [9–12], $f(T)$ [13,14], $f(G, T)$ [15], $f(R, G)$ [16,17], $f(Q)$ [18,19], $f(R, T)$ [20–22], and

[a] e-mails: adnan.malik@zjnu.edu.cn; adnan.malik@skt.umt.edu.pk; adnanmalik_chheena@yahoo.com
[b] e-mail: attiyashafaq10@gmail.com
[c] e-mail: fyalmofarrah@pnu.edu.sa (corresponding author)
[d] e-mails: farasat.shamir@nu.edu.pk; mfs24@leicester.ac.uk; farasat.shamir@gmail.com
[e] e-mail: wsalbalawi@pnu.edu.sa

Published online: 07 February 2025

$f(R,\varphi)$ [23] theories of gravity, where R represents the Ricci scalar and φ represents the scalar potential. These theories address the limitations of classical gravity and are particularly significant for explaining phenomena such as dark energy and the late-time acceleration of the universe [24]. The innovative frameworks provided by these theories contribute to unraveling the mechanisms underlying accelerated cosmic expansion. Buchdahl [25] introduced $f(R)$ gravity, where the Ricci scalar R is replaced by an arbitrary function $f(R)$. Building on this foundation, Capozziello et al. [26] examined the hydrostatic equilibrium of stellar structures using the Lane–Emden equation within the context of $f(R)$ gravity. Among recent advancements, $f(R,\varphi)$ gravity has gained particular prominence due to its ability to incorporate a scalar field φ, which generates a repulsive force analogous to the effects of dark energy. Capozziello and Laurentis [27] proposed the inclusion of a scalar function in the Einstein–Hilbert action and explored $f(R,\varphi)$ gravity in depth. Furthermore, Zubair and Kousar [28] extended this framework by presenting $f(R, R_{\alpha\beta}R^{\alpha\beta}, \varphi)$ gravity, investigating energy bounds in this context, and examining the thermodynamic laws of black holes [29].

In MTG, the study of compact stars provides a framework for understanding how deviations from general relativity influence the structure and stability of such objects. MTG allows for the exploration of phenomena such as anisotropic pressures, charge distribution, and non-standard energy conditions, offering new insights into the formation, stability, and evolution of compact stars. By examining these modified gravitational models, researchers can probe the effects of dark energy, dark matter, and gravitational modifications on the interior structure and behavior of stellar remnants, enhancing our understanding of astrophysical objects in the universe. Kalm et al. [30] examined compact objects with anisotropic matter using the Krori and Barua metric. Bhar et al. [31] explored solutions for anisotropic stars within noncommutative spacetime, highlighting the possibility of compact stars existing in higher-dimensional frameworks. Ilyas [32] analyzed the internal configuration of charged compact stars in the context of $f(G)$ gravity. Similarly, Zubair et al. [33] investigated the formation and stability of compact stars under $f(R,T)$ gravity. Abbas et al. [34] studied the physical properties of compact stars and derived equilibrium conditions in $f(G)$ gravity. Noureen et al. [35] focused on the dynamical instability of anisotropic gravitating systems in $f(R)$ gravity, concluding that higher-order curvature corrections could be effectively replaced by the $f(R)$ model. Malik along with his collaborators [36–38] investigated the dynamics of some stellar structures and moment of inertia in GR as well as modified theories of gravity.

Investigating the stability of compact stars is a crucial aspect of modern astrophysics, as it provides valuable insights into the evolution and dynamics of celestial objects. Compact objects are considered to be in equilibrium when the outward and inward forces are balanced. However, this equilibrium may be either stable or unstable. Within compact objects, fusion processes generate energy, producing outward pressure that counteracts gravitational collapse. However, when this energy is depleted, the inward forces prevail, leading to collapse and the formation of compact stars. Bondi [39] made significant contributions to the study of celestial object stability using the adiabatic criterion. Chandrasekhar [40] further advanced the analysis of compact object stability by applying Bondi's framework and incorporating the adiabatic index. To examine the influence of dissipation on the dynamical instability of a spherically symmetric fluid, Herrera et al. [41] conducted an analysis in both the Newtonian and relativistic regimes. Chan et al. [42] demonstrated that even a slight alteration in the anisotropy of the unperturbed fluid can substantially affect the system's stability in both Newtonian and relativistic contexts. In a subsequent study [43], the same researchers explored the impact of shearing forces and viscosity, finding that these factors enhance the fluid's stability in both the Newtonian and relativistic frameworks.

Herrera [44] was the pioneer who proposed the cracking technique to examine the behavior of the fluid inside a compact object when its equilibrium state is disturbed. Specifically, it addresses the point at which non-zero radial forces emerge within the configuration. In the context of this technique, cracking occurs when inwardly directed radial forces change sign at a specific point, i.e., $(\frac{\delta\Omega}{\delta\rho} < 0 \rightarrow \frac{\delta\Omega}{\delta\rho} > 0)$. Conversely, overturning refers to a situation where outwardly directed forces change sign from positive to negative, i.e., $(\frac{\delta\Omega}{\delta\rho} > 0 \rightarrow \frac{\delta\Omega}{\delta\rho} < 0)$. Prisco et al. [45] expanded on the cracking method by employing the Raychaudhuri equation to identify the necessary constraints for cracking. Herrera et al. [46] analyzed the effects of local anisotropy on the cracking of compact objects through a Jeans instability analysis. Herrera and Varela [47] proposed a technique to examine cracking in non-spherical systems by introducing axisymmetric disturbances within an ideal fluid configuration. Prisco et al. [48] analyzed cracking in self-gravitating compact objects by perturbing the local anisotropy. Abreu et al. [49] investigated cracking by employing perturbations in the local anisotropy and density of compact objects using both local and non-local equations of state (EoS). Abreu et al. [50] also explored the presence of cracking and utilized concepts related to density fluctuations and sound speeds. Azam et al. [51] investigated the effects of electromagnetic fields on the stability of charged compact objects using the cracking technique. Malik et al. [52–54] discussed the cracking technique by considering the anisotropic as well as isotropic stellar structures in different modiefied theories of gravity.

To avoid common misunderstandings about the stability and cracking in the literature, Herrera and Prisco [55] clar-

ified that both of these concepts are distinct, despite often being confused. They concluded that "stability" refers to the ability of a given fluid distribution to return to equilibrium after being disturbed. The fact that the speed of sound is not superluminal does not guarantee the stability of the object; it only ensures causality. "Cracking", in contrast, refers to the system's tendency to 'split' immediately after being displaced from equilibrium, with 'immediately' meaning on a timescale shorter than both the hydrostatic timescale and the thermal relaxation time. What happens subsequently whether the system enters a dynamic regime or returns to equilibrium is independent of the concept of cracking. However, the occurrence of cracking will affect the future evolution of the fluid configuration in either case. To determine whether cracking occurs, the system must be perturbed from its equilibrium state by applying fluctuations. In the original cracking paper [44], these fluctuations were assumed to be generic (of an 'unspecified' nature). The specific case of fluctuations associated with fluid compression was considered in [50]. In this latter case, confusion between cracking and stability may arise due to the relationship between the adiabatic index, the speed of sound, and stability. In simple words, In a system which is stable, i.e. a system that once removed from equilibrium comes back to it in a timescale of the order of hydrostatic time, cracking may occur or not, "or" after the occurrence of cracking the system may return to equilibrium (the system is stable) or enters into a dynamic regime (the system is unstable).

However, the primary focus of our study is to analyze the cracking and overturning phenomena that occur when a system departs from equilibrium due to perturbations. The concept of cracking, as discussed in our work, specially refers to the immediate tendency of the system to split following perturbation, independent of whether the system is ultimately stable or unstable. The layout of this manuscript is organized as follows: In Sect. 2, we derive the field equations and expressions for hydrostatic equilibrium within the $f(R,\varphi)$ gravity framework, and apply the Krori Barua metric [56]. In Sect. 3, we apply the LDP to all physical variables and develop the equation for radial forces to identify cracking and overturning points. In Sect. 4, we validate this technique using data from Her X-1, SAX J1808.4-3658, and 4U 1820-30, along with a graphical representation of radial forces. Finally, in Sect. 5, we present our concluding remarks, followed by the appendix and references.

2 Basic background of $f(R,\varphi)$ theory of gravity

The action is given as [57–59],

$$S=\frac{1}{2K}\int d^4x\sqrt{-g}\Big[f(R,\varphi)+w(\varphi)\varphi_{;\eta}\varphi^{;\eta}+L_m\Big], \quad (1)$$

where g and L_M are the determinants of the metric tensor $g_{\xi\eta}$ and the lagrangian function, respectively. Furthermore, R and $\varphi\equiv\varphi(r)$ represent Ricci scalar and scalar potential function, respectively. For the sake of simplicity, we use $\varphi(r)\equiv\varphi$, $f\equiv f(\mathcal{R},\varphi)$, and $w_\varphi\equiv w$. The field equations can be obtained by varying the action (1) with respect to $g_{\xi\eta}$ as

$$f_R R_{\xi\eta}-\frac{1}{2}\Big[f+w(\varphi)\varphi_{;\alpha}\varphi^{;\alpha}\Big]g_{\xi\eta}+w(\varphi)\varphi_{;\alpha}\varphi^{;\alpha} -f_{R;\xi\eta}+g_{\xi\eta}\Box f_R=kT_{\xi\eta}, \quad (2)$$

where $\Box\equiv\nabla^\mu\nabla^\lambda$ represents the D'Alembert operator and $f_R=\frac{\partial f}{\partial R}$. An alternative form of modified field equations in the shape of GR can be written as

$$G_{\xi\eta}=R_{\xi\eta}-\frac{1}{2}Rg_{\xi\eta}=\frac{1}{f_R}\Big[T^{(m)}_{\xi\eta}+T^{(D)}_{\xi\eta}\Big], \quad (3)$$

where, $T^m_{\xi\eta}$ is the usual energy momentum tensor for anisotropic matter configuration is illustrated as

$$T^{(m)}_{\xi\eta}=(\rho+p_t)u_\xi u_\eta-p_t g_{\xi\eta}+(p_r-p_t)\upsilon_\xi\upsilon_\eta, \quad (4)$$

where ρ, p_t, p_r denote the energy density, tangential pressure, and radial pressures, respectively. Additionally, $u_\xi=e^{a/2}\delta^0_\xi$ and $\upsilon_\eta=e^{b/2}\delta^1_\eta$ signify velocity 4-vectors. Moreover, $T^{(D)}_{\xi\eta}$ can be written as

$$T^D_{\xi\eta}=\frac{1}{f_R}\Big[-\frac{1}{2}g_{\xi\eta}Rf_R+\frac{1}{2}(f+w(\varphi)\varphi_{;\alpha}\varphi^{;\alpha})g_{\xi\eta} -w(\varphi)\varphi_{;\xi}\varphi_{;\eta}+f_{R;\xi\eta}-g_{\xi\eta}\Box f_R\Big]. \quad (5)$$

For our current work, we consider the spherically symmetric spacetime as

$$ds^2=e^{\lambda(r)}dt^2-e^{\zeta(r)}dr^2-r^2(d\theta^2+sin^2\theta d\varphi^2), \quad (6)$$

where $e^{a(r)}$ and $e^{b(r)}$ represent metric coefficients. After some manipulations, we get the following field equations as

$$G_{00}=\frac{e^\lambda}{f_R}\Big[\rho-\frac{1}{2}Rf_R+\frac{1}{2}f-\frac{1}{2}w(\varphi)\varphi'^2e^{-\zeta} +e^{-\zeta}f''_R+e^{-\zeta}\Big(\frac{\zeta'}{2}+\frac{2}{r}\Big)f'_R\Big], \quad (7)$$

$$G_{11}=\frac{e^\zeta}{f_R}\Big[p_r+\frac{1}{2}Rf_R-\frac{1}{2}f-\frac{1}{2}w(\varphi)\varphi'^2e^{-\zeta} -e^{-\zeta}\Big(\frac{\lambda'}{2}+\zeta'+\frac{2}{r}\Big)f'_R\Big], \quad (8)$$

$$G_{22}=\frac{r^2}{f_R}\Big[p_t+\frac{1}{2}Rf_R-\frac{1}{2}f+\frac{1}{2}w(\varphi)\varphi'^2e^{-\zeta} -e^{-\zeta}f''_R-e^{-\zeta}\Big(\frac{\lambda'}{2}+\frac{\zeta'}{2}+\frac{2}{r}\Big)f'_R\Big], \quad (9)$$

$$G_{33} = \frac{r^2 sin^2\theta}{f_R}\Big[p_t + \frac{1}{2}Rf_R - \frac{1}{2}f + \frac{1}{2}w(\varphi)\varphi'^2 e^{-\zeta} - e^{-\zeta}f_R'' - e^{-\zeta}\left(\frac{\lambda'}{2} + \frac{\zeta'}{2} + \frac{1}{r}\right)f_R'\Big]. \tag{10}$$

where $f_\varphi = \frac{\partial f}{\partial \varphi}$ and prime is derivatives with respect to radial coordinate "r". Moreover, the hydrostatic equilibrium equation can be obtained as

$$\begin{aligned}\frac{dp_r}{dr} &= e^{\zeta}f_R\Big[\frac{e^{-2\zeta}}{f_R}\Big(\frac{f - Rf_R}{2}e^{\zeta} - \frac{1}{2}w(\varphi)\varphi'^2 - \Big(\frac{\lambda'}{2} + \zeta' + \frac{2}{r}\Big)f_R'\Big]_{,1} \\ &- \frac{\rho\lambda'}{2} - \Big(\frac{\lambda'}{2} + \frac{2}{r} + \frac{f_R'R'}{f_R\rho'}\Big)p_r + \frac{2p_t}{r} \\ &+ e^{-\zeta}\Big(-\frac{\lambda'}{2} - \frac{2}{r}\Big)f_R'' \\ &+ e^{-\zeta}\Big(\frac{3}{4}\lambda'\zeta' + \frac{\lambda'^2}{4} + \frac{3\zeta'}{r} + \frac{2}{r^2} + \zeta'^2\Big)f_R' \\ &+ \zeta'\Big(\frac{f - Rf_R}{2}\Big) + e^{-\zeta}\Big(\frac{\lambda'}{2} + \frac{\zeta'}{2} + \frac{2}{r}\Big)w(\varphi)\varphi'^2,\end{aligned} \tag{11}$$

which implies to

$$\begin{aligned}\Omega &= -\frac{dp_r}{dr} + e^{\zeta}f_R\Big[\frac{e^{-2\zeta}}{f_R}\Big(\frac{f - Rf_R}{2}e^{\zeta} - \frac{1}{2}w(\varphi)\varphi'^2 - \Big(\frac{\lambda'}{2} + \zeta' + \frac{2}{r}\Big)f_R'\Big]_{,1} \\ &- \frac{\rho\lambda'}{2} - \Big(\frac{\lambda'}{2} + \frac{2}{r} + \frac{f_R'R'}{f_R\rho'}\Big)p_r + \frac{2p_t}{r} \\ &+ e^{-\zeta}\Big(-\frac{\lambda'}{2} - \frac{2}{r}\Big)f_R'' \\ &+ e^{-\zeta}\Big(\frac{3}{4}\lambda'\zeta' + \frac{\lambda'^2}{4} + \frac{3\zeta'}{r} + \frac{2}{r^2} + \zeta'^2\Big)f_R' \\ &+ \zeta'\Big(\frac{f - Rf_R}{2}\Big) + e^{-\zeta}\Big(\frac{\lambda'}{2} + \frac{\zeta'}{2} + \frac{2}{r}\Big)w(\varphi)\varphi'^2,\end{aligned} \tag{12}$$

where Ω represents the total force acting on a fluid element, appearing after perturbation, when the fluid is out of equilibrium.

3 Local density perturbation technique

This section formulates the equation for radial forces by integrating the concept of local density perturbation (LDP) into physical parameters. The LDP technique is a valuable tool for investigating how minor fluctuations in matter density influence gravitational behavior within the framework of modified gravity theories [60]. By analyzing small deviations from uniform density, this method enables the study of spacetime responses under various gravitational models. Such an approach offers insights into the behavior of gravity beyond classical theories, particularly in regimes of strong gravitational fields or near compact objects. It serves as a bridge between theoretical predictions and observed phenomena, especially in areas where traditional gravity theories fall short of providing a comprehensive explanation.

Additionally, this study assumes a density-dependent nature of these parameters while simultaneously considering the barotropic equation of state (EoS), expressed as $p_r = p_r(\rho)$ and $p_t = p_t(\rho)$. Cracking occurs when the radial forces $\frac{\delta\Omega}{\delta\rho}$, which are directed inward ($\frac{\delta\Omega}{\delta\rho} < 0$), change sign to become $\frac{\delta\Omega}{\delta\rho} > 0$. Conversely, overturning occurs when the radial forces, initially directed outward ($\frac{\delta\Omega}{\delta\rho} > 0$), change sign. Next, we introduce the density perturbation $\rho \to \rho + \delta\rho$ into the physical parameters as follows:

$$\rho(\rho + \delta\rho) = \rho(\rho) + \delta\rho, \tag{13}$$

$$\rho'(\rho + \delta\rho) = \rho'(\rho) + \frac{\rho''}{\rho'}\delta\rho, \tag{14}$$

$$p_r(\rho + \delta\rho) = p_r(\rho) + \frac{dp_r}{d\rho}\delta\rho = p_r(\rho) + v_r^2\delta\rho, \tag{15}$$

$$\begin{aligned}\frac{dp_r}{dr}(\rho + \delta\rho) &= \frac{dp_r}{dr} + \Big[\frac{d}{dr}\Big(\frac{dp_r}{d\rho}\Big) + \frac{d^2\rho}{dr^2}\Big(\frac{dp_r}{d\rho}\Big).\frac{dr}{d\rho}\Big] \\ &= \frac{dp_r}{dr} + v_r'^2 + v_r^2.\rho''(\rho')^{-1},\end{aligned} \tag{16}$$

$$p_t(\rho + \delta\rho) = p_t(\rho) + \frac{dp_t}{d\rho}\delta\rho = p_t(\rho) + v_t^2\delta\rho, \tag{17}$$

$$f_R(\rho + \delta\rho) = f_R(\rho) + \frac{R'}{\rho'}f_R'\delta\rho, \tag{18}$$

$$f_R'(\rho + \delta\rho) = f_R'(\rho) + \frac{R'}{\rho'}f_R''\delta\rho, \tag{19}$$

$$f_R''(\rho + \delta\rho) = f_R''(\rho) + \frac{R'}{\rho'}f_R'''\delta\rho, \tag{20}$$

$$f(\rho + \delta\rho) = \Big[\frac{R'}{\rho'}f_R + \frac{\varphi'}{\rho'}f_\varphi\Big]\delta\rho, \tag{21}$$

$$f_\varphi(\rho + \delta\rho) = f_\varphi(\rho) + \frac{\varphi'}{\rho'}f_\varphi'\delta\rho, \tag{22}$$

$$R'(\rho + \delta\rho) = R'(\rho) + \frac{R''}{\rho'}\delta\rho, \tag{23}$$

$$w(\rho + \delta\rho) = w(\rho) + \frac{\varphi'}{\rho'}w'\delta\rho, \tag{24}$$

$$w'(\rho + \delta\rho) = w'(\rho) + \frac{\varphi'}{\rho'}w''\delta\rho, \tag{25}$$

$$\varphi'(\rho + \delta\rho) = \varphi'(\rho) + \frac{\varphi''}{\rho'}\delta\rho, \tag{26}$$

Table 1 Estimated values of X, Y, M, R of compact stars

Compact stars	$M(M_\odot)$	R/km	$\alpha = M/R$	X/km^{-2}	Y/km^{-2}	Z_s
Her X-I	0.88 $M_\odot$	7.7	0.168	0.010 906 441 192	0.0042673646183	0.23
SAXJ1808.4-3658	1.435 $M_\odot$	7.07	0.299	0.01823156974	0.014880115692	0.57
4U 1820-30	2.25 $M_\odot$	10.0	0.332	0.010906441192	0.009880 9523811	0.073

$$\varphi''(\rho+\delta\rho) = \varphi''(\rho) + \frac{\varphi'''}{\rho'}\delta\rho. \tag{27}$$

Further, v_r^2 and v_t^2 signify the radial and tangential sound speeds, respectively, and are expressed as

$$v_r^2 = \frac{dp_r}{d\rho}\ ,\ v_t^2 = \frac{dp_t}{d\rho}. \tag{28}$$

Now, the radial forces $\frac{\delta\Omega}{\delta\rho}$ arising from perturbing the system can be determined by employing the local density perturbation technique. By expanding Eq. (12), its perturbed form is obtained as follows:

$$\begin{aligned}\Omega = \Omega_0\Big(&\rho,\ \rho',\ p_r,\ p_r',\ p_t,\ f_R,\ f_R',\ f_R'',\ R',\\ &\times f,\ f_\varphi,\ \varphi',\ \varphi'',\ w(\varphi),\ w'(\varphi)\Big) + \delta\Omega,\end{aligned} \tag{29}$$

where

$$\begin{aligned}\delta\Omega = &\frac{\partial\Omega}{\partial\rho}\delta\rho + \frac{\partial\Omega}{\partial\rho'}\delta\rho' + +\frac{\partial\Omega}{\partial p_r}\delta p_r\\ &+\frac{\partial\Omega}{\partial p_r'}\delta p_r' + \frac{\partial\Omega}{\partial p_t}\delta p_t + \frac{\partial\Omega}{\partial f_R}\delta f_R + \frac{\partial\Omega}{\partial f_R'}\delta f_R' + \frac{\partial\Omega}{\partial f_R''}\delta f_R''\\ &+\frac{\partial\Omega}{\partial R'}\delta R' + \frac{\partial\Omega}{\partial f}\delta f + \frac{\partial\Omega}{\partial f_\varphi}\delta f_\varphi + \frac{\partial\Omega}{\partial f_\varphi'}\delta f_\varphi'\\ &+\frac{\partial\Omega}{\partial\varphi'}\delta\varphi' + \frac{\partial\Omega}{\partial\varphi''}\delta\varphi'' + \frac{\partial\Omega}{\partial w}\delta w + \frac{\partial\Omega}{\partial w'}\delta w'.\end{aligned} \tag{30}$$

Equation (30) further modifies to

$$\begin{aligned}\frac{\delta\Omega}{\delta\rho} = &+\frac{\partial\Omega}{\partial\rho'}\Big(\rho''(\rho')^{-1}\Big) + \frac{\partial\Omega}{\partial p_r}\Big(v_r^2\Big)\\ &+\frac{\partial\Omega}{\partial p_r'}\Big(v_r'^2 + v_r^2\,\rho''(\rho')^{-1}\Big)\\ &+\frac{\partial\Omega}{\partial p_t}\Big(v_t^2\Big) + \frac{\partial\Omega}{\partial f_R}\Big(f_R'\frac{R'}{\rho'}\Big)\\ &+\frac{\partial\Omega}{\partial f_R'}\Big(f_R''\frac{R'}{\rho'}\Big) + \frac{\partial\Omega}{\partial f_R''}\Big(f_R'''\frac{R'}{\rho'}\Big) + \frac{\partial\Omega}{\partial R'}\Big(\frac{R''}{\rho'}\Big)\\ &+\frac{\partial\Omega}{\partial f}\Big(f_R\frac{R'}{\rho'} + f_\varphi\frac{\varphi'}{\rho'}\Big) + \frac{\partial\Omega}{\partial f_\varphi}\Big(f_\varphi'\frac{\varphi'}{\rho'}\Big)\\ &+\frac{\partial\Omega}{\partial\varphi'}\Big(\frac{\varphi''}{\rho'}\Big) + \frac{\partial\Omega}{\partial\varphi''}\Big(\frac{\varphi'''}{\rho'}\Big)\\ &+\frac{\partial\Omega}{\partial w}\Big(\frac{w'\varphi'}{\rho'}\Big) + \frac{\partial\Omega}{\partial w'}\Big(\frac{w''\varphi'}{\rho'}\Big).\end{aligned} \tag{31}$$

It can be noticed that the subsequent partial derivatives of Eq. (31) can be seen in Eqs. (A1)–(A15) as written in Appendix.

4 Discussion

This section explores the effects of LDP on $f(R,\varphi)$ theory of gravity. To investigate these effects, we utilize Eq. (31), which describes the perturbed state of the system. The primary objective is to identify the cracking and overturning points by examining the changes in the signs of the perturbed states induced by LDP. For this analysis, we adopt the $f(R,\varphi)$ gravity model [57] as

$$f(R,\varphi) = \varphi(R + \alpha R^2). \tag{32}$$

We assume that $w(\varphi) = v_0\varphi^n$ and $\varphi = r^\beta$, where α, β, and n are non-zero constants. To validate our proposed approach within the framework of the modified $f(R,\varphi)$ theory of gravity, we analyze the compact stars Her X-1, SAX J 1808-3658, and 4U 1820-30. Table 1 lists the constants, radii, and masses for each star under consideration. Furthermore, Figs. 1, 2 and 3 in the subsequent subsections provide a graphical representation of $\frac{\delta\Omega}{\delta\rho}$ as a function of the model parameter β for the selected compact stars.

4.1 Star 1: Her X -1

Her X-1 was first discovered by Tananbaum and collaborators [61], who identified a new pulsating X-ray source in the constellation Hercules, characterized by a pulse period of 1.24 s and an orbital period of 1 day. Later, in 1995, Li et al. [62] suggested that Her X-1 is a strange star based on the $M-R$ relationship of strange stars.

Figure 1 presents the plots of $\frac{\delta\Omega}{\delta\rho}$ for Her X-1. These plots reveal that overturning occurs within the interval $\beta \in (0, 0.05]$, as shown in Fig. 1a–d. Additionally, the figures indicate that cracking points are present in the interval $\beta \in (0, 0.14]$, highlighting disruptions in radial forces under perturbations.

Moreover, Fig. 1e–i demonstrate that neither cracking nor overturning occurs within the interval $\beta \in (0.14, 1]$, suggesting that the star's configuration remains stable and resistant to disruptions in this range. Table 2 summarizes the specific

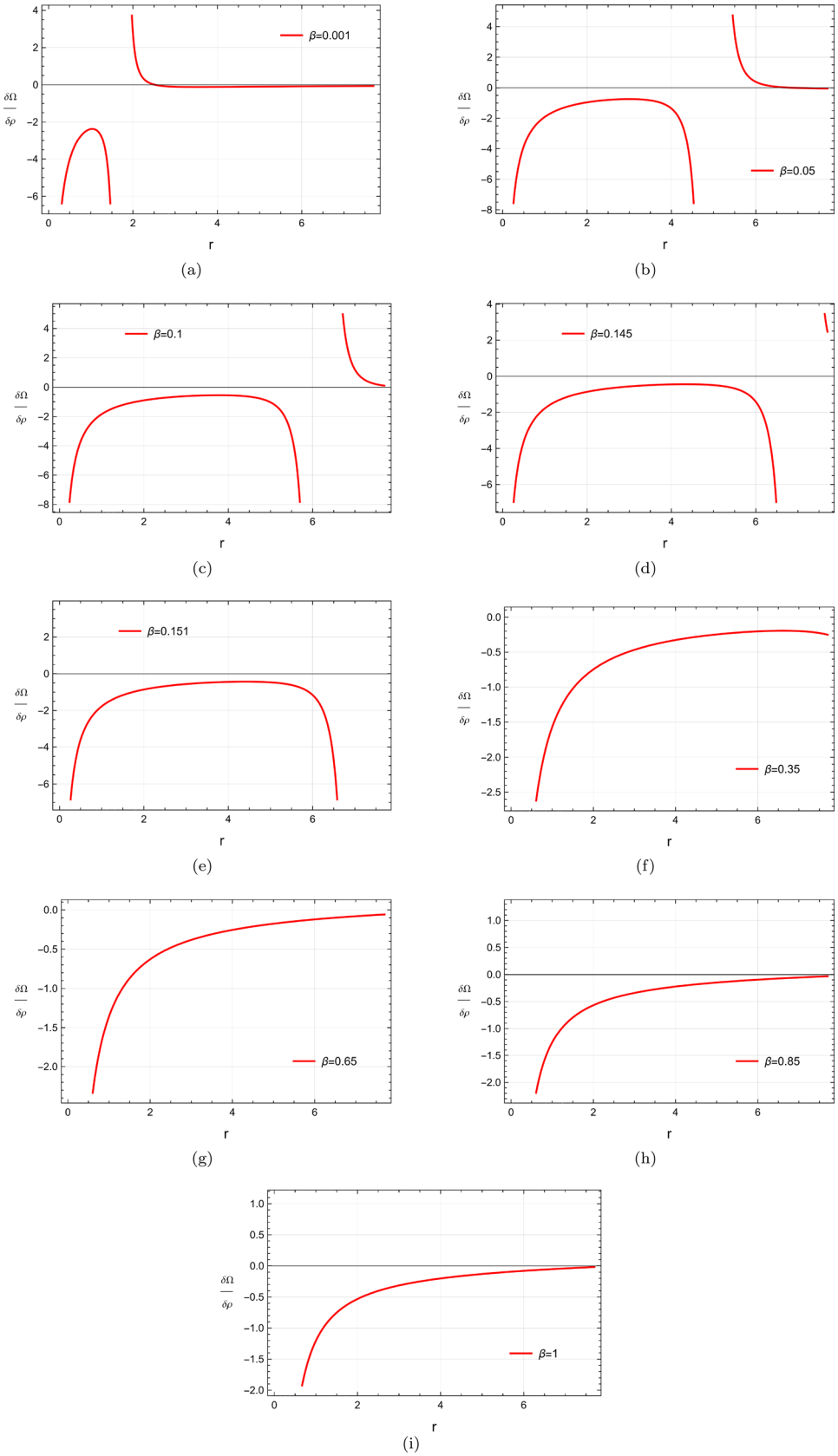

Fig. 1 Plots of $\frac{\delta\Omega}{\delta\rho}$ for Her X-1: $X = 0.0069062764281\,\mathrm{km}^2$, $Y = 0.0042673646183\,\mathrm{km}^2$, $n = -1.5$, $v_0 = 0.5$, $\alpha = 0.168$

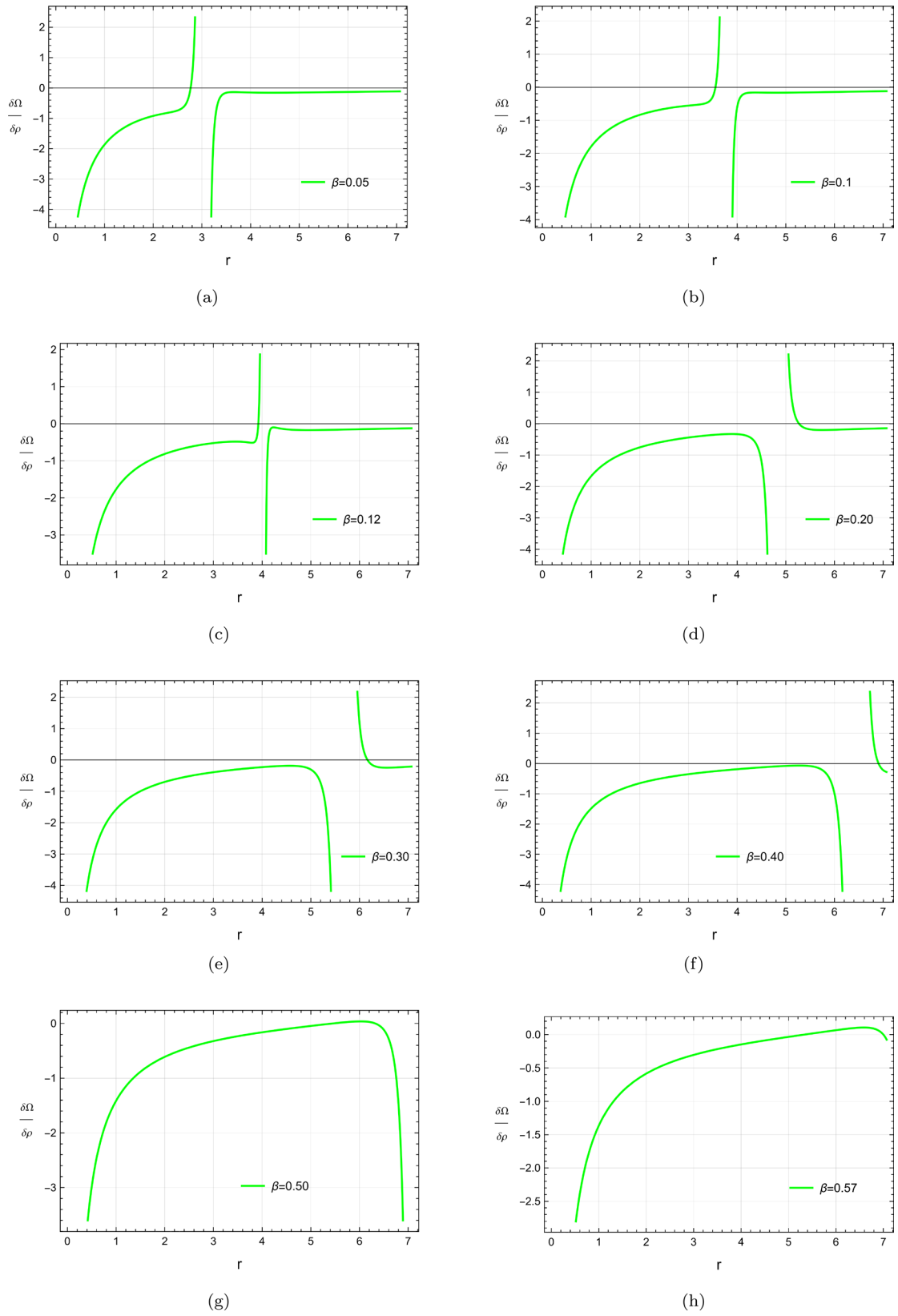

Fig. 2 Plots of $\frac{\delta\Omega}{\delta\rho}$ for SAXJI808.4-3658: $X = 0.0182315697401\,\mathrm{km}^2$, $Y = .014880115692\,\mathrm{km}^2$, $n = -1.5$, $v_0 = 0.5$, $\alpha = 0.299$

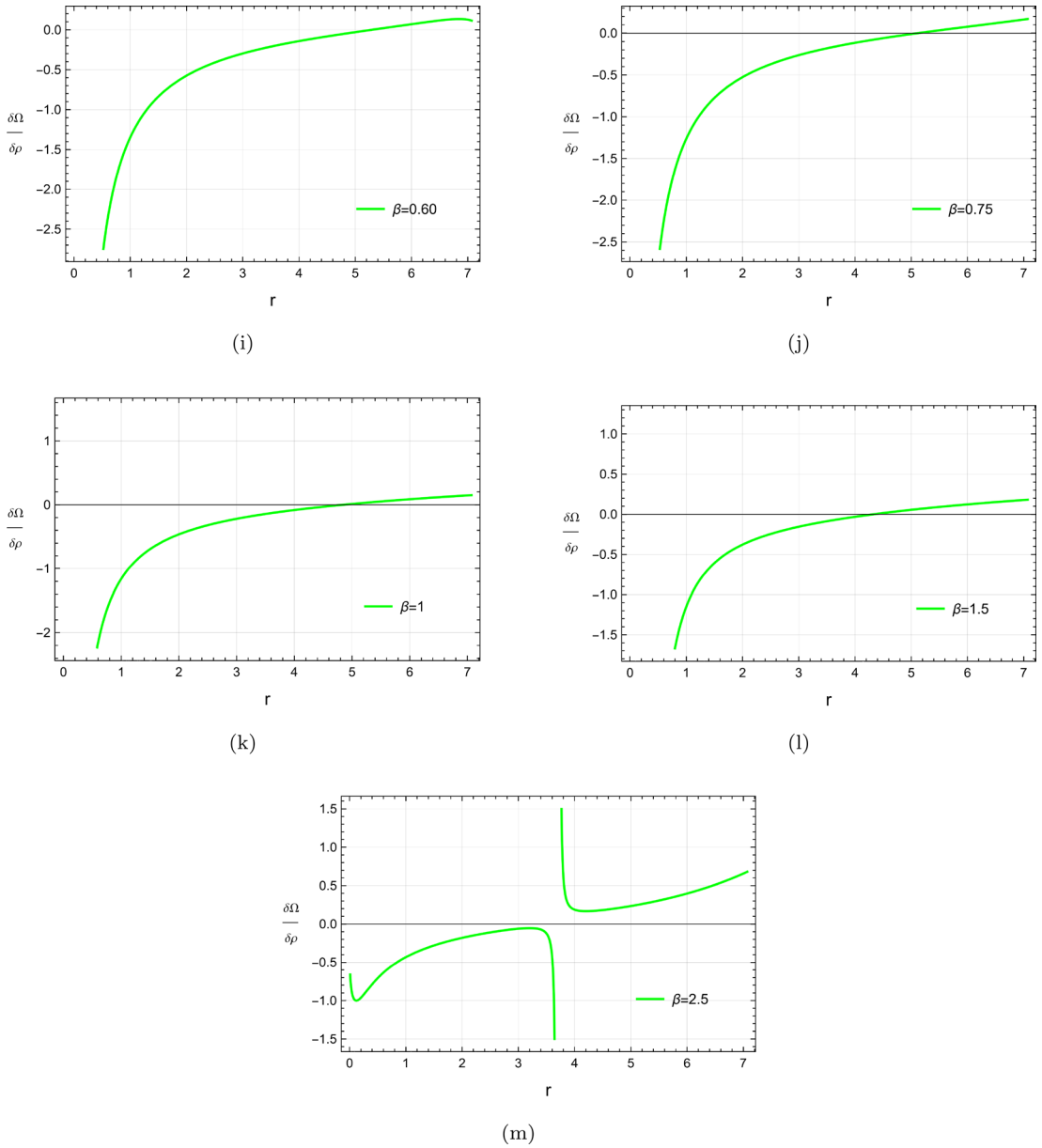

Fig. 2 continued

values of β at which the star exhibits cracking and overturning points.

4.2 Star 2: SAXJ1808.4-3658

Zand et al. [63] identified SAX J1808.4-3658 as a compact neutron star with an orbital period of 2 h. Subsequently, Li et al. [64] proposed that SAX J1808.4-3658 is a candidate for a strange star based on its $M - R$ relation.

We have plotted $\frac{\delta\Omega}{\delta\rho}$ for SAX J1808.4-3658 by considering different values of β, as shown in Fig. 2. The plots in Fig. 2a–h demonstrate that overturning occurs within the

Table 2 Cracking and overturning points in Her X-1

β	Cracking points (r (km))	Overturning points (r (km))
0.001	r = 1.95879	r = 2.47562
0.05	r = 5.44825	r = 7.03499
0.1	r = 6.70768	–
0.145	–	–
0.15	–	–
0.35	–	–
0.65	–	–
0.85	–	–
1	–	–

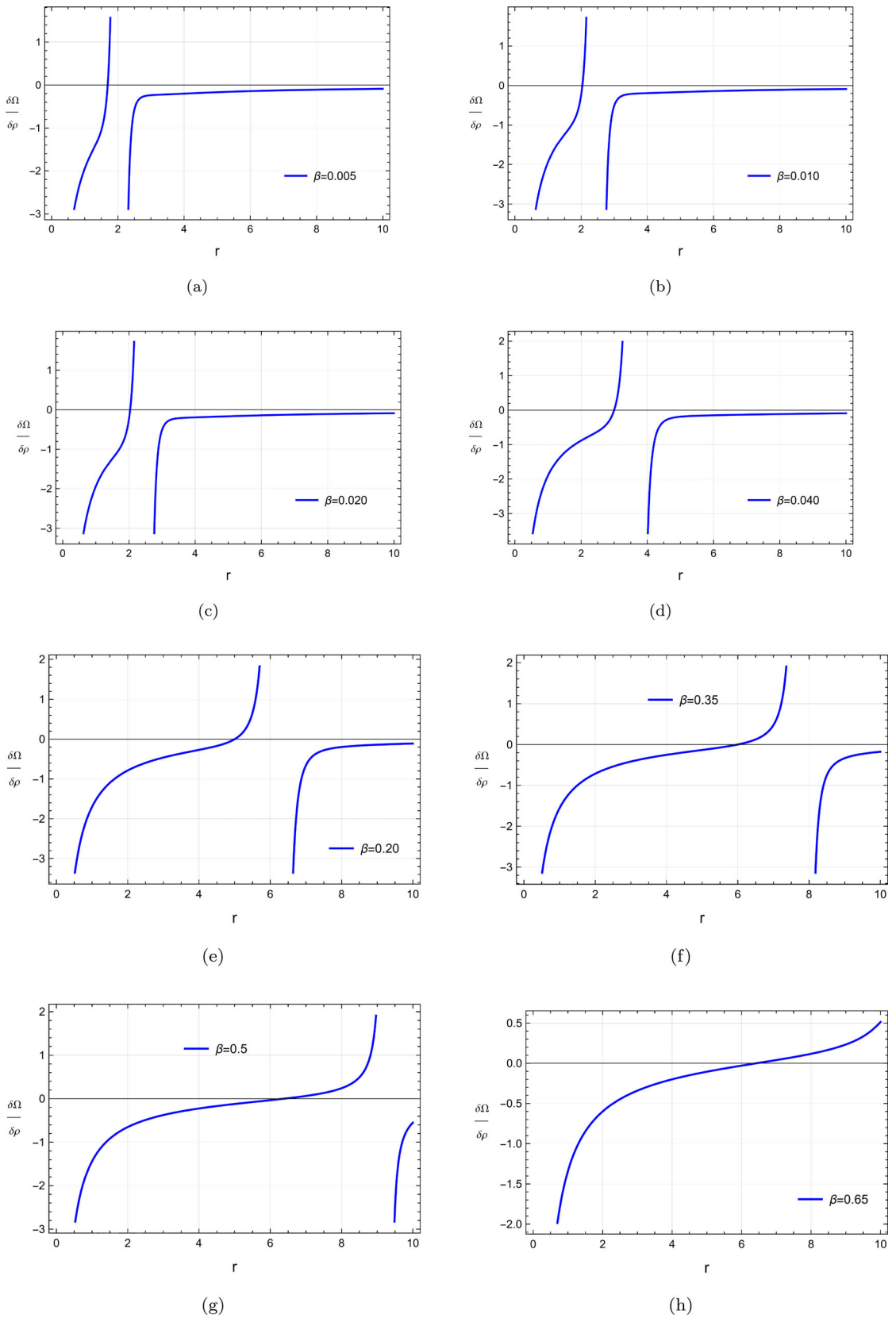

Fig. 3 Plots of $\frac{\delta\Omega}{\delta\rho}$ for 4U1820-30: $X = 0.0109064411921\,\mathrm{km}^2$, $Y = 0.0098809523811\,\mathrm{km}^2$, $n = -1.5$, $v_0 = 0.5$, $\alpha = 0.332$

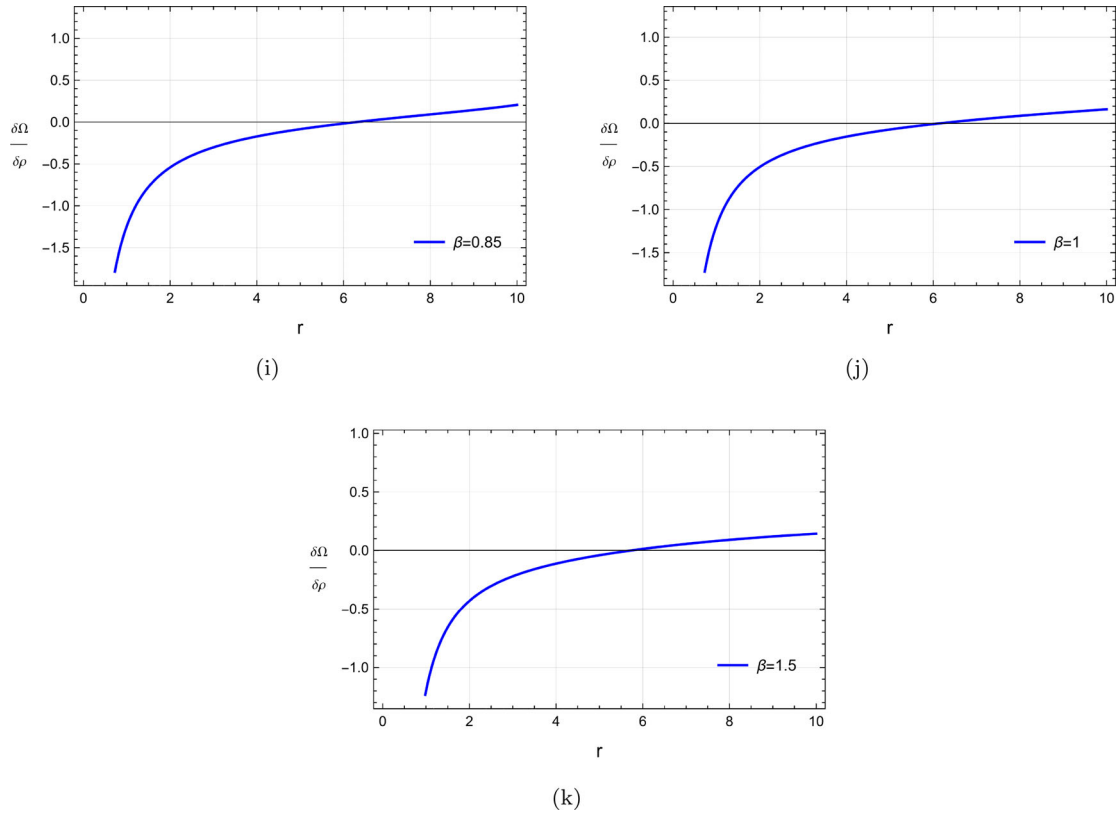

Fig. 3 continued

interval $\beta \in (0, 0.57]$. Furthermore, Fig. 2a–m reveal that cracking points appear within $\beta \in (0, 3]$.

These findings highlight disruptions within the respective intervals, underscoring the system's sensitivity to applied perturbations. Table 3 provides a summary of the values of β at which the star exhibits cracking and overturning points.

4.3 Star 3: 4U 1820-30

Guver et al. [65] analyzed the spectral data from thermonuclear bursts and reported the mass and radius of 4U 1820-30 to be $1.58 \pm 0.06\, M_{\odot}$ and 9.11 ± 0.40 km, respectively.

We have plotted $\frac{\delta\Omega}{\delta\rho}$ over a wide range of the model parameter β for 4U 1820-30, as shown in Fig. 3. Figure 3a–g indicate that both cracking and overturning occur within the interval $\beta \in (0, 0.5]$. Within this range, overturning points appear exclusively in $\beta \in (0, 0.5]$.

In contrast, Fig. 3a–k illustrate that 4U 1820-30 exhibits cracking points throughout $\beta \in (0, 3]$. These findings reveal disturbances in the configuration across the specified intervals, highlighting the system's sensitivity to the applied perturbations. Table 4 provides a summary of the values of β at which the star exhibits cracking and overturning points.

Table 3 Cracking and overturning points in SAXJ1808.4-3658

β	Cracking points (r (km))	Overturning points (r (km))
0.05	r = 2.77706	r = 3.18340
0.1	r = 3.553319	r = 3.88898
0.12	r = 3.92738	r = 4.16722
0.20	r = 5.07131	r = 5.29391
0.30	r = 5.94913	r = 6.21129
0.40	r = 6.73561	r = 6.93221
0.50	r = 5.64871	r = 6.42326
0.57	r = 5.59862	r = 7.00442
0.60	r = 5.58511	–
0.75	r = 5.47697	–
1	r = 4.96189	–
1.5	r = 4.45909	–
2.5	r = 3.75403	–

5 Conclusion

In this paper, we investigated the phenomenon of cracking within the framework of the modified $f(R, \varphi)$ theory of gravity. The primary objective was to examine the conditions under which cracking and overturning occur, analyze their dependence on physical parameters such as density pertur-

Table 4 Cracking and overturning points in 4U 1820-30

β	Cracking points (r (km))	Overturning points (r (km))
0.005	r = 1.65991	r = 2.27967
0.010	r = 2.05934	r = 3.05045
0.020	r = 2.46891	r = 3.30982
0.040	r = 3.38050	r = 4.02068
0.20	r = 5.09601	r = 6.61629
0.35	r = 6.15279	r = 8.15512
0.5	r = 6.72753	r = 9.49001
0.65	r = 6.79087	–
0.85	r = 6.52745	–
1	r = 6.53527	–
1.5	r = 6.11803	–
1.85	r = 6.01232	–

bations, and understand their implications for the behavior of compact stars in modified gravity scenarios.

This goal was achieved by considering an anisotropic matter distribution with spherical symmetry and deriving the field equations, as presented in Eqs. (7)–(10). Additionally, we derived the hydrostatic equilibrium equation using the principle of energy conservation and adopted the spacetime coefficients proposed by Krori and Barua [56].

To further our analysis, we formulated the radial force equation by incorporating local density perturbations (LDP) into the physical parameters while accounting for a barotropic equation of state (EoS). The main focus was to evaluate cracking and overturning points by examining the changes in the signs of the perturbed state, as expressed in Eq. (31), under the influence of LDP.

For validation, we employed the model $f(R, \varphi) = \varphi(R + \alpha R^2)$, as proposed in [57]. Three compact stars Her X-1, SAX J1808 3658, and 4U 1820 30 were selected for this analysis. The previous section provides the plots of radial forces $\frac{\delta\Omega}{\delta\rho}$ for each star, along with accompanying observations. Tables 2 and 4 summarize the positions of cracking and overturning for each considered star.

In conclusion, the following key findings have been derived from our analysis:

- Her X-1 exhibits overturning and cracking within the intervals $\beta \in (0, 0.05]$ and $\beta \in (0, 0.14]$, respectively. For $\beta \in (0.14, 1]$, neither cracking nor overturning phenomena are observed.
- SAX J1808.4-3658 exhibits overturning and cracking points within $\beta \in (0, 0.57]$ and $\beta \in (0, 3]$, respectively. These observations indicate disruptions within the specified intervals, highlighting the system's sensitivity to the applied perturbations.
- For 4U 1820-30, overturning points are observed within $\beta \in (0, 0.5]$, while cracking points appear at $\beta \in (0, 3]$. These results underscore disruptions in the configuration across the respective intervals, emphasizing the sensitivity of the system to perturbations.

Based on the analysis, it can be concluded that the occurrence of cracking and overturning phenomena is linked to disturbances in the configuration, causing a deviation from hydrostatic equilibrium. Our findings reveal that all the stars under consideration are sensitive to local density perturbations, which result in the formation of cracking and overturning points within these stars. This study is significant as it identifies regions prone to localized density disruptions, providing valuable insights into the structural behavior of compact stars within modified gravity frameworks.

Acknowledgements The authors extend their appreciation to the Deanship of Scientific Research and Libraries in Princess Nourah bint Abdulrahman University for funding this research work through the Research Group project, Grant No. (RG-1445-0036).

Data Availibility Statement My manuscript has no associated data. [Author's comment: This is a theoretical study and no experimental data.].

Code Availability Statement My manuscript has no associated code/software. [Author's comment: Code/Software sharing not applicable to this article as no code/software was generated or analysed during the current study.]

Declarations

Conflict of interest The authors have declared that they have no interest of conflict.

Funded by SCOAP[3].

Appendix

$$\frac{\partial\Omega}{\partial\rho} = -Yr. \tag{A1}$$
$$\frac{\partial\Omega}{\partial\rho'} = \frac{f'_R R'}{f_R(\rho')^2}$$

$$+e^{-Xr^2}\Big(-\frac{2XrR'}{(\rho')^2}-\frac{2R'}{r(\rho')^2}-\frac{YrR'}{(\rho')^2}\Big)f_R''$$
$$+\frac{fR'f_R'}{2f_R(\rho')^2}+\frac{e^{-Xr^2}w(\varphi)\varphi'^2R'f_R'}{2(\rho')^2f_R}$$
$$+\frac{e^{-Xr^2}\Big(2Xr+Yr+\frac{2}{r}\Big)(f_R')^2R'}{(\rho')^2f_R}. \tag{A2}$$

$$\frac{\partial\Omega}{\partial p_r}=-\Big(Yr+\frac{2}{r}-\frac{f_R'R'}{f_R\rho'}\Big). \tag{A3}$$

$$\frac{\partial\Omega}{\partial p_r'}=-1. \tag{A4}$$

$$\frac{\partial\Omega}{\partial p_t}=\frac{2}{r}. \tag{A5}$$

$$\frac{\partial\Omega}{\partial f_R}=\Big(\frac{-f_R^2R'}{(f_R)\rho'}\Big)p_r+\frac{fR'f_R'}{2(f_R)^2\rho'}+\frac{e^{-Xr^2}w(\varphi)\varphi'^2R'f_R'}{2(f_R)^2\rho'}$$
$$+\Big(2Xr+Yr+\frac{2}{r}\Big)\frac{e^{-Xr^2}(f_R')^2R'}{(f_R)^2\rho'}. \tag{A6}$$

$$\frac{\partial\Omega}{\partial f_R'}=\Big(\frac{R'}{f_R\rho'}\Big)p_r-XYr^2e^{-Xr^2}+Y^2r^2e^{-Xr^2}$$
$$-4X^2r^2e^{-Xr^2}+\frac{2}{r^2}e^{-Xr^2}+Ye^{-Xr^2}-\frac{fR'}{2f_R\rho'}$$
$$-\frac{e^{-Xr^2}w(\varphi)\varphi'^2R'}{2f_R\rho'}-\Big(2Xr+Yr+\frac{2}{r}\Big)\frac{2e^{-Xr^2}f_R'R'}{f_R\rho'}. \tag{A7}$$

$$\frac{\partial\Omega}{\partial f_R''}=e^{-Xr^2}\Big(-Yr-\frac{2}{r}+\frac{YrR'}{\rho'}+\frac{2XrR'}{\rho'}+\frac{2R'}{r\rho'}\Big). \tag{A8}$$

$$\frac{\partial\Omega}{\partial R'}=\Big(\frac{f_R'}{f_R\rho'}\Big)p_r+e^{-Xr^2}\Big(\frac{Yr}{\rho'}+\frac{2Xr}{\rho'}+\frac{2}{r\rho'}\Big)f_R''$$
$$+\Big(-\frac{f}{2f_R\rho'}-\frac{e^{-Xr^2}w(\varphi)\varphi'^2}{2f_R\rho'}\Big)f_R'$$
$$-\Big(2Xr+Yr+\frac{2}{r}\Big)\frac{e^{-Xr^2}(f_R')^2}{f_R\rho'}+\frac{f(\varphi)\varphi'}{2}. \tag{A9}$$

$$\frac{\partial\Omega}{\partial f}=-\frac{R'f_R'}{2f_R\rho'}. \tag{A10}$$

$$\frac{\partial\Omega}{\partial f(\varphi)}=\frac{\varphi'}{2}. \tag{A11}$$

$$\frac{\partial\Omega}{\partial\varphi'}=\frac{e^{-Xr^2}w(\varphi)\varphi'f_R'}{f_R\rho'}+2e^{-Xr^2}\Big(Yr-Xr+\frac{2}{r}\Big)w(\varphi)\varphi'$$
$$+\frac{3e^{-Xr^2}w'(\varphi)\varphi'^2}{2}+e^{-Xr^2}w(\varphi)\varphi''+\frac{f(\varphi)}{2}. \tag{A12}$$

$$\frac{\partial\Omega}{\partial\varphi''}=e^{-Xr^2}w(\varphi)\varphi'. \tag{A13}$$

$$\frac{\partial\Omega}{\partial w}=\frac{e^{-Xr^2}w(\varphi)\varphi'^2R'f_R'}{2f_R\rho'}+e^{-Xr^2}w(\varphi)\varphi''\varphi'$$
$$+e^{-Xr^2}\Big(Yr-Xr+\frac{2}{r}\Big)\varphi'^2. \tag{A14}$$

$$\frac{\partial\Omega}{\partial w'}=\frac{e^{-Xr^2}\varphi'''}{2}. \tag{A15}$$

$$\begin{aligned}\rho=&\frac{1}{2}e^{-2r^2X}r^{-4+\beta}(2e^{2r^2X}(r^2-2\alpha)\\&+e^{r^2X}(-2r^4X(-2+\beta)+r^{2+\beta}(r^\beta)^mw_0\beta^2\\&+8\alpha(3-3\beta+\beta^2)+r^2(8X\alpha(-4+\beta)-2(1+\beta+\beta^2)))\\&+4\alpha(-5+r^8Y(4X^3-3X^2Y-2XY^2+Y^3)+6\beta\\&-2\beta^2+2r^6(4X^3+3Y^3+3XY^2(3+\beta)-3X^2Y(6+\beta))\\&+2r^2(-3Y\beta(1+\beta)+X(2+5\beta+2\beta^2))\\&-r^4(4X^2(8+3\beta)-2XY(24+14\beta+\beta^2)\\&+Y^2(3+10\beta+2\beta^2)).\end{aligned} \tag{A16}$$

$$\begin{aligned}p_r=&\frac{1}{2}e^{-2r^2X}r^{-4+\beta}+(-2e^{2r^2X}(r^2-2\alpha)\\&+e^{r^2X}(8\alpha(3-2\beta)+r^{2+\beta}(r^\beta)^mw_0\beta^2\\&+r^2(2-16X\alpha(-2+\beta)+4\beta-8Y\alpha\beta)\\&+2r^4(2X\beta+Y(2+\beta))\\&+4\alpha(-7-r^8Y(-8X^3+5X^2Y+2XY^2+Y^3)\\&+4\beta-2r^2(-7Y\beta+2X(4+\beta))\\&+2r^6(2X+Y)(4X^2+Y^2(1+\beta)-XY(7+\beta))\\&+r^4(X^2(4-8\beta)+4XY(-8+\beta)+Y^2(11+10\beta)).\end{aligned} \tag{A17}$$

$$\begin{aligned}p_t=&\frac{1}{2}e^{-2r^2X}r^{-4+\beta}(-4e^{2r^2X}\alpha+e^{r^2X}(2r^6Y(-X+Y)\\&-r^{2+\beta}(r^\beta)^mw_0\beta^2-8\alpha(3-4\beta+\beta^2)\\&+r^2(-8Y\alpha(-3+\beta)-8X\alpha(-1+\beta)+2\beta^2)\\&+2r^4(X(-1+\beta)+Y(2+\beta))\\&-4\alpha(-7+r^8(X-Y)^2(4X-Y)Y\\&+8\beta-2\beta^2+2r^6(X-Y)\\&\times(4X^2+Y^2(4+\beta)-XY(17+3\beta)\\&-r^4(4X^2(5+3\beta)-2XY(19+15\beta+\beta^2)\\&+Y^2(11+14\beta+2\beta^2)+r^2(-2Y(-3+\beta+3\beta^2)\\&+X(-6+6\beta+4\beta^2))).\end{aligned} \tag{A18}$$

$$\begin{aligned}v_r^2=&(-2e^{2r^2X}(-2\alpha(-4+\beta)+r^2(-2+\beta))\\&+e^{r^2X}(-2r^{4+\beta}(r^\beta)^mw_0X\beta^2\\&+r^{2+\beta}(r^\beta)^mw_0\beta^2(-2+(2+m)\beta)\\&-8\alpha(12-11\beta+2\beta^2)\end{aligned}$$

$$
\begin{aligned}
&- 4r^6X(2X\beta + Y(2+\beta))\\
&- 2r^2((-2+\beta)(-1-2\beta+4Y\alpha\beta)\\
&+ 8X\alpha(7-6\beta+\beta^2))\\
&+ 2r^4(16X^2\alpha(-2+\beta) + Y\beta(2+\beta)\\
&+ 2X(-1-2\beta+4Y\alpha\beta+\beta^2)))\\
&- 4\alpha(-28 + 4r^{10}XY(8X^3 - 5X^2Y - 2XY^2 - Y^3)\\
&+ 23\beta - 4\beta^2\\
&+ r^8(64X^4 + Y^4(4+\beta) - 8X^3Y(14+3\beta)\\
&+ 2XY^3(8+5\beta) + X^2Y^2(-20+13\beta))\\
&+ 2r^2(-7Y(-2+\beta)\beta + 2X(-15+6\beta+\beta^2))\\
&- 2r^6(8X^3(1+3\beta)\\
&+ XY^2(-32-23\beta+\beta^2) + Y^3(2+3\beta+\beta^2)\\
&- 2X^2Y(-22+11\beta+\beta^2)) + r^4(-4XY(-22+\beta)\beta\\
&- Y^2\beta(11+10\beta)\\
&+ 4X^2(-16-5\beta+2\beta^2))))/\\
&(2e^{2r^2X}(-2\alpha(-4+\beta) + r^2(-2+\beta))\\
&+ e^{r^2X}(4r^6X^2(-2+\beta) - 2r^{4+\beta}(r^\beta)^m w_0 X\beta^2\\
&+ r^{2+\beta}(r^\beta)^m w_0\beta^2(-2+(2+m)\beta)\\
&+ 2r^4X(2 - 8X\alpha(-4+\beta) + 4\beta + \beta^2)\\
&+ 8\alpha(-12+15\beta-7\beta^2+\beta^3)\\
&+ 2r^2(2+\beta+\beta^2-\beta^3-4X\alpha(-2+\beta^2))\\
&- 4\alpha(-20 + 4r^{10}XY(4X^3 - 3X^2Y - 2XY^2 + Y^3)\\
&+ 29\beta - 14\beta^2 + 2\beta^3\\
&+ r^8(32X^4 - Y^4(4+\beta) + 2XY^3(16+\beta)\\
&- 4X^3Y(40+7\beta) + 3X^2Y^2(28+9\beta))\\
&+ r^4(-2XY\beta(36+26\beta+\beta^2) + Y^2\beta(3+10\beta+2\beta^2)\\
&+ 4X^2(4+18\beta+7\beta^2))\\
&- 2r^6(3Y^3(2+\beta) + 4X^3(18+7\beta)\\
&+ XY^2(24+35\beta+7\beta^2) - X^2Y(132+80\beta+7\beta^2)\\
&- 2r^2(3Y\beta(2+\beta-\beta^2) + X(6-20\beta+5\beta^2+2\beta^3)))).
\end{aligned}
\tag{A19}
$$

$$
\begin{aligned}
v_t^2 = &(-4e^{2r^2X}\alpha(-4+\beta) + e^{r^2X}(4r^8X(X-Y)Y\\
&+ 2r^{4+\beta}(r^\beta)^m w_0 X\beta^2\\
&- r^{2+\beta}(r^\beta)^m w_0\beta^2(-2+(2+m)\beta)\\
&- 8\alpha(-12+19\beta-8\beta^2+\beta^3)\\
&+ r^6(-4X^2(-1+\beta) - 6XY(2+\beta) + 2Y^2(2+\beta))\\
&+ 2r^4(8XY\alpha(-3+\beta) + 8X^2\alpha(-1+\beta)\\
&- X\beta(1+\beta) + Y\beta(2+\beta))\\
&+ 2r^2((-2+\beta)(-4Y\alpha(-3+\beta)+\beta^2)\\
&+ 4X\alpha(4-5\beta+\beta^2)))\\
&+ 4\alpha(-28 + 4r^{10}X(X-Y)^2(4X-Y)Y\\
&+ 39\beta - 16\beta^2 + 2\beta^3)\\
&+ r^8(X-Y)(32X^3 + 13XY^2(4+\beta)\\
&- Y^3(4+\beta) - 4X^2Y(38+7\beta)\\
&- 2r^6(4X^3(12+7\beta) - Y^3(8+6\beta+\beta^2)\\
&- X^2Y(118+87\beta+7\beta^2)\\
&+ XY^2(64+57\beta+8\beta^2)) + r^4(Y^2\beta(11+14\beta+2\beta^2)\\
&+ 4X^2(-6+11\beta+7\beta^2)\\
&- 2XY(-12+23\beta+27\beta^2+\beta^3)t)\\
&- 2r^2(Y(-6+5\beta+5\beta^2-3\beta^3) + X(20\\
&- 25\beta + 3\beta^2 + 2\beta^3))))/\\
&(2e^{2r^2X}(-2\alpha(-4+\beta) + r^2(-2+\beta))\\
&+ e^{r^2X}(4r^6X^2(-2+\beta)\\
&- 2r^{4+\beta}(r^\beta)^m w_0 X\beta^2\\
&+ r^{2+\beta}(r^\beta)^m w_0\beta^2(-2+(2+m)\beta)\\
&+ 2r^4X(2 - 8X\alpha(-4+\beta) + 4\beta + \beta^2)\\
&+ 8\alpha(-12+15\beta-7\beta^2+\beta^3)\\
&+ 2r^2(2+\beta+\beta^2-\beta^3-4X\alpha(-2+\beta^2)))\\
&- 4\alpha(-20 + 4r^{10}XY(4X^3 - 3X^2Y - 2XY^2 + Y^3)\\
&+ 29\beta - 14\beta^2 + 2\beta^3\\
&+ r^8(32X^4 - Y^4(4+\beta) + 2XY^3(16+\beta)\\
&- 4X^3Y(40+7\beta) + 3X^2Y^2(28+9\beta))\\
&+ r^4(-2XY\beta(36+26\beta+\beta^2)\\
&+ Y^2\beta(3+10\beta+2\beta^2) + 4X^2(4+18\beta+7\beta^2))\\
&- 2r^6(3Y^3(2+\beta) + 4X^3(18+7\beta)\\
&+ XY^2(24+35\beta+7\beta^2) - X^2Y(132+80\beta+7\beta^2)\\
&- 2r^2(3Y\beta(2+\beta-\beta^2)\\
&+ X(6-20\beta+5\beta^2+2\beta^3))))).
\end{aligned}
\tag{A20}
$$

References

1. D. Wang et al., Observational constraints on a logarithmic scalar field dark energy model and black hole mass evolution in the Universe. Eur. Phys. J. C **83**(7), 1–14 (2023)
2. A.V. Filippenko, A.G. Riess, Results from the high-z supernova search team. Phys. Rep. **307**(1–4), 31–44 (1998)
3. M.F. Shamir et al., Dark $f(R,\phi,X)$ universe with Noether symmetry. Theor. Math. Phys. **205**(3), 1692–1705 (2020)
4. A.G. Riess et al., Observational evidence from supernovae for an accelerating universe and a cosmological constant. Astron. J. **116**(3), 1009 (1998)

5. D.N. Spergel et al., First-year Wilkinson Microwave Anisotropy Probe (WMAP)* observations: determination of cosmological parameters. Astrophys. J. Suppl. Ser. **148**(1), 175 (2003)
6. J. Mehra, One month in the history of the discovery of general relativity theory. Found. Phys. Lett. **11**, 41–60 (1998)
7. V. Venkatesha et al., Yukawa–Casimir wormholes in the framework of $f(R)$ gravity. Eur. Phys. J. C **84**(8), 834 (2024)
8. S.A. Mardan et al., Spherically symmetric generating solutions in $f(R)$ theory. Eur. Phys. J. Plus **138**(9), 782 (2023)
9. T. Naz et al., Finch–Skea Stellar structures obeying Karmarkar condition in modified $f(G)$ gravity. Chin. J. Phys. **89**, 871–883 (2024)
10. A. Rashid et al., A comprehensive study of Bardeen stars with conformal motion in $f(G)$ gravity. Eur. Phys. J. C **83**(11), 997 (2023)
11. Z. Yousaf et al., Stability of anisotropy pressure in self-gravitational systems in $f(G)$ gravity. Axioms **12**(3), 257 (2023)
12. Z. Yousaf et al., Bouncing cosmology with 4D-EGB gravity. Int. J. Theor. Phys. **62**(7), 155 (2023)
13. C.C. Chalavadi et al., Exploration of GUP-corrected Casimir wormholes in extended teleparallel gravity with matter coupling. Nucl. Phys. B **1006**, 116644 (2024)
14. M.Z. Bhatti et al., Energy density inhomogeneities with self-gravitating charged fluid in modified teleparallel gravity. Int. J. Geom. Methods Mod. Phys. **21**(9), 2450171 (2024)
15. T. Naz et al., Relativistic configurations of Tolman stellar spheres in $f(G,T)$ gravity. Int. J. Geom. Methods Mod. Phys. **20**(13), 2350222 (2023)
16. T. Naz et al., Evolving embedded traversable wormholes in $f(R,G)$ gravity: a comparative study. Phys. Dark Univ. **42**, 101301 (2023)
17. T. Naz et al., Traversable wormhole solutions utilizing the Karmarkar condition in $f(R,G)$ gravity. Commun. Theor. Phys. **76**(12), 125402 (2024)
18. P. Bhar et al., Physical characteristics and maximum allowable mass of hybrid star in the context of $f(Q)$ gravity. Eur. Phys. J. C **83**(7), 1–19 (2023)
19. P. Bhar et al., Impact of f (Q) gravity on anisotropic compact star model and stability analysis. Chin. J. Phys. **88**, 839–856 (2024)
20. T. Naz et al., Physical behavior of anisotropic quark stars in modified $f(R,T)$ gravity. Int. J. Theor. Phys. **63**(3), 78 (2024)
21. Z. Asghar et al., Study of embedded class-I fluid spheres in $f(R,T)$ gravity with Karmarkar condition. Chin. J. Phys. **83**, 427–437 (2023)
22. I. Fayyaz et al., Fate of charged wormhole structures utilizing Karmarkar approach. New Astron. **112**, 102255 (2024)
23. Z. Asghar et al., Comprehensive analysis of relativistic embedded class-I exponential compact spheres in $f(R,\phi)$ gravity via Karmarkar condition. Commun. Theor. Phys. **75**(10), 105401 (2023)
24. S. Capozziello, Curvature quintessence. Int. J. Mod. Phys. D **11**(04), 483–491 (2002)
25. H.A. Buchdahl, Non-linear Lagrangians and cosmological theory. Mon. Not. Roy. Astron. Soc. **150**(1), 1–8 (1970)
26. S. Capozziello et al., Hydrostatic equilibrium and stellar structure in $f(R)$ gravity. Phys. Rev. D-Part. Fields Gravit. Cosmol. **83**(6), 064004 (2011)
27. S. Capozziello, M. De Laurentis, Extended theories of gravity. Phys. Rep. **509**(4–5), 167–321 (2011)
28. M. Zubair, F. Kousar, Cosmological reconstruction and energy bounds in $f(R,\ R_{\alpha\beta}R^{\alpha\beta},\varphi)$ gravity. Eur. Phys. J. C **76**, 1–13 (2016)
29. M. Zubair et al., Thermodynamics in $f(R,\ R_{\alpha\beta}R^{\alpha\beta},\varphi)$ theory of gravity. Phys. Dark Univ. **14**, 116–125 (2016)
30. M. Kalam et al., Anisotropic strange star with de Sitter spacetime. Eur. Phys. J. C **72**, 1–7 (2012)
31. P. Bhar et al., Possibility of higher-dimensional anisotropic compact star. Eur. Phys. J. C **75**(5), 190 (2015)
32. M. Ilyas, Charged compact stars in $f(G)$ gravity. Eur. Phys. J. C **78**(9), 757 (2018)
33. M. Zubair et al., Possible formation of compact stars in $f(R,T)$ gravity. Astrophys. Space Sci. **361**(1), 8 (2016)
34. G. Abbas et al., Anisotropic compact stars in f (G) gravity. Astrophys. Space Sci. **357**, 1–11 (2015)
35. I. Noureen et al., Impact of extended Starobinsky model on evolution of anisotropic, vorticity-free axially symmetric sources. J. Cosmol. Astropart. Phys. **2015**(02), 033 (2015)
36. A. Malik et al., Effects of charge on perfect fluid stellar structure and moment of inertia in $f(R)$ gravity. Int. J. Theor. Phys. **64**(1), 11 (2025)
37. A. Malik et al., Dynamics of some compact structures and moment of inertia in $f(R,T)$ gravity. Int. J. Geom. Methods Mod. Phys. **21**(10), 2440025–341 (2024)
38. A. Malik, M. Farasat Shamir, Exact perfect fluid interior solutions and slowly rotating relativistic stars. Eur. Phys. J. Plus **139**(5), 448 (2024)
39. H. Bondi, Massive spheres in general relativity. Proc. Roy. Soc. Lond. Ser. A Math. Phys. Sci. **282**(1390), 303–317 (1964)
40. S. Chandrasekhar, Dynamical instability of gaseous masses approaching the Schwarzschild limit in general relativity. Phys. Rev. Lett. **12**(4), 114 (1964)
41. L. Herrera, G. Le Denmat, N.O. Santos, Dynamical instability for non-adiabatic spherical collapse. Mon. Not. Roy. Astron. Soc. **237**(1), 257–268 (1989)
42. R. Chan, L. Herrera, N.O. Santos, Dynamical instability for radiating anisotropic collapse. Mon. Not. Roy. Astron. Soc. **265**(3), 533–544 (1993)
43. R. Chan, L. Herrera, N.O. Santos, Dynamical instability for shearing viscous collapse. Mon. Not. Roy. Astron. Soc. **267**(3), 637–646 (1994)
44. L. Herrera, Cracking of self-gravitating compact objects. Phys. Lett. A **165**(3), 206–210 (1992)
45. A. Di Prisco et al., Tidal forces and fragmentation of self-gravitating compact objects. Phys. Lett. A **195**(1), 23–26 (1994)
46. L. Herrera, N.O. Santos, Local anisotropy in self-gravitating systems. Phys. Rep. **286**(2), 53–130 (1997)
47. L. Herrera, V. Varela, Transverse cracking of self-gravitating bodies induced by axially symmetric perturbations. Phys. Lett. A **226**(3–4), 143–149 (1997)
48. A. Di Prisco, L. Herrera, V. Varela, Cracking of homogeneous self-gravitating compact objects induced by fluctuations of local anisotropy. Gen. Relativ. Gravit. **29**(10), 1239–1256 (1997)
49. H. Abreu, H. Hernández, L.A. Núñez, Cracking of self-gravitating compact objects with local and non local equations of state. Journal of Physics: Conference Series (Vol. 66, No. 1, p. 012038). IOP Publishing (2007)
50. H. Abreu, H. Hernández, L.A. Núnez, Sound speeds, cracking and the stability of self-gravitating anisotropic compact objects. Class. Quantum Gravity **24**(18), 4631 (2007)
51. M. Azam, S.A. Mardan, M.A. Rehman, Cracking of compact objects with electromagnetic field. Astrophys. Space Sci. **359**, 1–8 (2015)
52. A. Malik et al., A comprehensive discussion for the identification of cracking points in $f(R)$ theories of gravity. Eur. Phys. J. C **83**(8), 1–22 (2023)
53. A. Malik et al., Stability analysis of anisotropic stellar structures in Rastall theory of gravity utilizing cracking technique. Chin. J. Phys. **89**, 613–627 (2024)
54. A. Malik et al., Stability analysis of isotropic compact stars in $f(R,T)$ gravity utilizing cracking technique. Chin. J. Phys. **90**, 1101–1116 (2024)
55. L. Herrera, A. Di Prisco, Cracking and complexity of self-gravitating dissipative compact objects. Phys. Rev. D **109**(6), 064071 (2024)

56. K.D. Krori, J. Barua, A singularity-free solution for a charged fluid sphere in general relativity. J. Phys. A Math. Gen. **8**(4), 508 (1975)
57. A. Malik et al., Anisotropic strange quintessence stars in modified $f(R, \phi)$ theory of gravity. Int. J. Geom. Methods Mod. Phys. **21**(10), 2440003 (2024)
58. A. Malik et al., Investigation of charged stellar structures in $f(R, \phi)$ gravity using Reissner–Nordstrom geometry. Int. J. Geom. Methods Mod. Phys. **21**(5), 2450099–22 (2024)
59. A. Malik et al., Charged stellar structure in $f(R, \phi)$ gravity admitting Chaplygin equation of state. Int. J. Geom. Methods Mod. Phys. **21**, 2450086 (2024)
60. A. Malik et al., Development of local density perturbation technique to identify cracking points in $f(R, T)$ gravity. Eur. Phys. J. C **83**(9), 1–17 (2023)
61. H. Tananbaum et al., Discovery of a periodic pulsating binary X-ray source in Hercules from UHURU. Astrophys. J. **174**, L143 (1972)
62. X.-D. Li et al., Is HER X-1 a strange star? Astron. Astrophys. **303**, L1 (1995)
63. J.J.M. Zand et al., Discovery of the X-ray transient SAX J1808. 4-3658, a likely low mass X-ray binary. arXiv preprint arXiv:astro-ph/9802098 (1998)
64. X.-D. Li et al., Is SAX J1808. 4-3658 a strange star? Phys. Rev. Lett. **83**(19), 3776 (1999)
65. T. Güver et al., The mass and radius of the neutron star in 4U 1820-30. Astrophys. J. **719**(2), 1807 (2010)